Volume 19, Number 1, 2026. pp. 85-95

Jordan Journal of Physics

ARTICLE

Landau Theory Analysis of Dielectric Properties of $BiFeO_3$ Ferroelectric Thin Films

Ahmad M. Alrub[a], **Qais S. Al-Horani**[a,b], **Ayat M. Alsiedat**[c,d], **J. M. Khoshman**[a], **Emad A. M. Farrag**[e], **Hatem A. Al Ameryeen**[a], **Bilal Abdallah Sadeh**[e] and **Abdel-Baset M. A. Ibrahim**[f]

[a] *Department of Physics, Al-Hussein Bin Talal University, Ma'an 71111, Jordan.*

[b] *Department of Marine Sciences, Al-Balqa' Applied University, Aqaba, Jordan.*

[c] *Department of Chemistry, Al-Hussein Bin Talal University, Ma'an 71111, Jordan.*

[d] *Department of Chemistry, The University of Jordan, Amman, Jordan.*

[e] *Department of Physics, College of Science, Jouf University, Skaka, Saudi Arabia.*

[f] *Faculty of Applied Sciences, Universiti Teknologi MARA (UiTM), 40450 Shah Alam, Selangor, Malaysia.*

DOI: **https://doi.org/10.47011/19.1.9**

Received on: 30/07/2025; *Accepted on: 12/01/2026*

Abstract: The dielectric properties and phase transition behavior of $BiFeO_3$ (BFO) ferroelectric thin films are explored using Landau-Ginzburg-Devonshire theory, accounting for polarization variation near the surfaces. The Euler-Lagrange (E-L) equation is numerically solved to model switching properties under an applied step electric field. Dielectric hysteresis loops are generated for various thicknesses and temperatures, revealing a critical thickness of 0.452 nm, revealing a critical thickness of 0.452 nm, which highlights BFO's potential for nanoscale applications. The electric susceptibility is computed for several film thicknesses, showing a high value (~10^4) near the transition temperature, even for a film thickness of 1 nm. At room temperature, the susceptibility increases as the film thickness decreases, reaching a value of 51.7 at 30 °C for the 1 nm film. These findings are consistent with experimental observations that report an average dielectric constant of approximately ε~50 in a single BFO crystal. Additionally, at room temperature, the calculated average polarization for BFO films with thicknesses between 1 nm and 6 nm falls in the range 0.50–0.55 C/m², indicating a relatively high value compared with other ferroelectric materials.

Keywords: Ferroelectricity, Landau theory, Phase transitions, $BiFeO_3$ thin films, Dielectric properties.

1. Introduction

BFO has been extensively studied for its multiferroic properties, which can be exploited at room temperature [1], an uncommon and advantageous trait among multiferroic materials. Reports on bulk BFO have yielded contradictory results regarding its remanent polarization and dielectric properties. Some studies report that bulk BFO exhibits significant remanent polarization and strong dielectric properties [2, 3]. These findings are supported by Local-Spin-Density and first-principles calculations [4, 5]. However, other experimental studies have reported significantly lower values of remanent polarization and dielectric constants in bulk BFO [6, 7]. These discrepancies have been attributed to factors such as the presence of secondary phases [8–10], high leakage currents, which pose a major challenge for practical applications [11–13], and low permittivity [14]. Nonstoichiometry and defects that are difficult to control during

Corresponding Author: Ahmad Musleh Alrub **Email**: AhmadAlrub@ahu.edu.jo

bulk synthesis also contribute to these discrepancies. The thermodynamic instability of the perovskite phase at high temperatures, which can lead to the formation of non-perovskite secondary phases, further complicates the realization of bulk BFO with ideal properties [8, 9]. On the theoretical side, inconsistencies arise from the sensitivity of the polarization to the structural distortions in the BFO lattice, which are not always accurately captured in the theoretical models [15, 16]. This gap between theory and experiment highlights the challenges in synthesizing bulk BFO with consistently high multiferroic performance [15].

Thin films benefit from enhanced properties due to strain effects [17, 18], epitaxial growth techniques, and the ability to better control stoichiometry and phase purity during film deposition [19–24]. Consequently, BFO thin films have demonstrated significantly higher remanent polarization and dielectric constants compared to their bulk counterparts [19, 16, 25–28]. This high remanent polarization of BFO thin films at room temperature makes them promising candidates for advanced applications in data storage, sensors, and spintronic devices [29]. The structural integrity and optical properties of BFO films, including a rhombohedral structure and a bandgap of approximately 2.33 eV, contribute to their effectiveness in electronic applications [30]. This paper focuses on the intrinsic dielectric properties of BFO thin films, aiming to explore the mechanisms underlying their ferroelectric behavior as influenced by film thickness and temperature. Understanding these mechanisms is essential for advancing the application of BFO in nanoscale devices, particularly in developing monolayer structures with reliable ferroelectricity, even at ultrathin dimensions.

From a theoretical perspective, the phase transitions and dielectric properties of BFO have been investigated using complementary approaches, including first-principles calculations, density functional theory (DFT), and phenomenological Landau theory. First-principles and DFT methods provide atomistic insight into electronic structure, while Landau-type models offer an efficient macroscopic framework for describing ferroelectric behavior in thin films. First-principles calculations offer accurate insights by solving the fundamental equations of quantum mechanics, and have, for example, revealed BFO's semiconducting nature, multiferroic behavior, and potential for spintronic applications [31]. DFT provides an efficient method for calculating electronic structures and predicting material properties, with studies detailing BFO's electronic band structures and confirming its dielectric relaxation phenomena, influenced by growth conditions [32].

However, while first-principles and DFT approaches are powerful, these methods often require significant computational resources and are more complex in capturing long-range interactions in thin films. Landau theory, meanwhile, offers a phenomenological framework for describing phase transitions and polarization behavior, particularly valuable for understanding ferroelectric properties at the macroscopic scale. Landau-type phenomenological theory has been extensively applied to study the physical properties of single-domain ferroelectric thin films with perovskite structure [33–37]. For example, Maren Daraktchiev et al. utilized a Landau potential expanded up to $P6$ to analyze domain wall properties in multiferroic systems with coupled order parameters [38]. Similarly, Vanderbilt and Cohen [39] demonstrated that expanding the Landau potential up to the eighth order is necessary to describe low-symmetry phases in ferroelectric perovskites.

This manuscript uses the Landau potential (up to the eighth order) to investigate phase transitions and dielectric properties of BFO films across varying thicknesses and temperatures. By analyzing dielectric hysteresis loops and susceptibility, the study provides a detailed understanding of BFO's ferroelectric behavior, highlighting its size- and temperature-dependent properties. This work could serve as an effective tool for guiding the experimental development of nanoscale ferroelectric devices for advanced applications in electronics and spintronics. In the following sections, we first present the theoretical framework, detailing the application of Landau theory to model phase transitions and dielectric properties of BFO thin films. This is followed by a discussion of the results, which explores polarization profiles, dielectric hysteresis loops, and susceptibility across various BFO film thicknesses and temperatures. Finally, we conclude with key findings.

2. Theory

The room-temperature phase of BFO is rhombohedral, with space group R3c and point group 3m, where ferroelectric polarization occurs along the [111] pseudocubic direction [40, 41]. Around 825 °C, BFO undergoes a first-order transition to a high-temperature β phase, accompanied by a sudden volume contraction and a peak in the dielectric constant, suggesting a ferroelectric-to-paraelectric transition [42, 43]. While there is some debate regarding the exact symmetry of the β phase above 825°C, it is generally accepted to be centrosymmetric [44–46]. The low-symmetry rhombohedral phase of BFO is characterized by a spontaneous polarization vector $P = (P_1, P_2, P_3)$, serving as the order parameter to describe the domain configuration and thermodynamic energies of the ferroelectric BFO single crystal.

We assume a freestanding BFO thin film of thickness L, extending along the z-axis from $z = -L/2$ to $z = (+L)/2$, under stress-free conditions. This allows us to isolate the intrinsic properties of the film without the influence of external uniaxial stress, which would otherwise induce symmetry changes from rhombohedral ($P_x = P_y = P_z$) to monoclinic ($P_x = P_y \neq P_z$). Our focus is on polarization behavior in the absence of such external effects. The polarization and related physical quantities vary as a function of z. Under short-circuited boundary conditions with ideal metallic electrodes, the depolarization field is strongly screened. Several experimental and theoretical studies on BFO capacitor structures have shown that high electrical conductivity of the electrodes and finite conductivity of BFO [1] itself substantially reduce the internal depolarizing field [47, 48]. Therefore, for the present study, we assume that the depolarization field is negligible. We note that this is a common approximation in LGD modeling of well-screened ferroelectric films. Nevertheless, we acknowledge that in real experimental systems incomplete screening can modify the polarization profile, and this represents a limitation of the present idealized model.

At room temperature, BFO exhibits a long-range magnetic order characterized by an incommensurate spin cycloid with a very long repeat distance of 62–64 nm [49]. In this cycloidal structure, the spins of the antiferromagnetically ordered sublattices rotate gradually, creating a spiral pattern. This results in BFO being a G-type antiferromagnet with no net magnetic moment below its Néel temperature of 370 °C [49]. However, a weak magnetization of 0.3 emu/g arises due to a small canting of the spins, induced by the Dzyaloshinskii–Moriya interaction, where the ferroelectric polarization breaks the center of symmetry and causes a slight deviation in the spin alignment [50, 51]. High magnetic fields, doping, or epitaxial strain can disrupt the cycloid, leading to the recovery of the canted state and its associated weak remnant magnetization [52, 53]. Given the negligible intrinsic magnetization of BFO thin films, we can disregard its effect in our calculations. For static effects, particularly in calculating the critical temperatures and dielectric properties of films due to the enhancement or suppression of polarization at the surfaces, the Tilley–Zeks (T-Z) model [54] is utilized as an extension of the Landau–Devonshire theory of bulk ferroelectrics. Based on this model, the total Landau free energy function (G_{total}) of ferroelectric phase under a stress-free freestanding BFO thin film includes contributions from the bulk free energy density (G_{bulk}), the gradient volume energy density (G_{grad}) accounting for the inhomogeneity due to variations in polarization (P) across the film thickness, the electric volume free energy density (G_{elec}), and the surface energy (G_{surf}) [54–56].

$$G_{total} = \int_{-\frac{L}{2}}^{\frac{L}{2}} \left(G_{bulk} + G_{grad} + G_{elec}\right) dV + G_{surf} \quad (1)$$

The polarization components of the uniaxial BFO film vary depending on the direction of the applied electric field. For our calculations, we assume an external electric field (E_z) is applied in the z-direction, normal to the film's surface. Consequently, we focus on determining the z-component of polarization (P_z).

$$G_{grad} = \gamma \left(\frac{dP}{dz}\right)^2 \quad (2)$$

$$G_{elec} = -E_z \hat{k}.\vec{P} = -E_z P_z \quad (3)$$

$$G_{surf} = \frac{\gamma}{2\delta}\left(P_{-z}^2 + P_{+z}^2\right) \quad (4)$$

Where γ determines the correlation energy and δ is the extrapolation length [57]. Here, P_{-z} and P_{+z} represent the z-components of the polarization at film surfaces located at $z = \mp L/2$. The bulk free energy density G_{bulk} is given by [56, 58];

$$G_{bulk} = \alpha_1(P_x^2 + P_y^2 + P_z^2) + \alpha_{11}\left(P_x^4 + P_y^4 + P_z^4\right) + \alpha_{12}\left(P_x^2P_y^2 + P_y^2P_z^2 + P_z^2P_x^2\right) + \alpha_{111}\left(P_x^6 + P_y^6 + P_z^6\right) + \alpha_{112}\left[P_x^2\left(P_y^4 + P_z^4\right) + P_y^2(P_z^4 + P_x^4) + P_z^2\left(P_y^4 + P_x^4\right)\right] + \alpha_{123}\left(P_x^2P_y^2P_z^2\right) + \alpha_{1111}\left(P_x^8 + P_y^8 + P_z^8\right) + \alpha_{1112}\left[P_x^6\left(P_y^2 + P_z^2\right) + P_y^6(P_z^2 + P_x^2) + P_z^6\left(P_y^2 + P_x^2\right)\right] + \alpha_{1122}\left(P_x^4P_y^4 + P_y^4P_z^4 + P_z^4P_x^4\right) + \alpha_{1123}\left(P_x^4P_y^2P_z^2 + P_y^4P_x^2P_z^2 + P_z^4P_y^2P_x^2\right) \quad (5)$$

Where α_1, α_{ij}, α_{ijk} and α_{ijkl} are the Landau coefficients with their values listed in Table A1 in Appendix A [56]. According to Landau-phenomenological theory, only the coefficient α_1 associated with the quadratic term of the order parameters depends on temperature, while the higher-order coefficients α_{ij}, α_{ijk} and α_{ijkl} are assumed to be temperature-independent. The rhombohedral phase of BFO is stable when $G_{total} < 0$, with a spontaneous polarization vector $P_x = \pm P_y = \pm P_z$. Under these conditions, Eq. (5) becomes:

$$G_{bulk} = 3\alpha_1P_z^2 + 3(\alpha_{11} + \alpha_{12})P_z^4 + (3\alpha_{111} + 6\alpha_{112} + \alpha_{123})P_z^6 + (3\alpha_{1111} + 6\alpha_{1112} + 3\alpha_{1122} + 3\alpha_{1123})P_z^8 \quad (6)$$

where $\alpha_2 = 3\alpha_1$, $\alpha_4 = 3(\alpha_{11} + \alpha_{12})$, $\alpha_6 = 3\alpha_{111} + 6\alpha_{112} + \alpha_{123}$, and $\alpha_8 = 3\alpha_{1111} + 6\alpha_{1112} + 3\alpha_{1122} + 3\alpha_{1123}$. The values of the coefficients α_2 α_4, α_6 and α_8 are calculated and listed in Table A2 in Appendix A. For the thin film, the fundamental assumption is that the equilibrium profile $P(z)$ corresponds to the minimization of the total free energy G_{total} Eq. (1). Thus, (z) is obtained as the solution to the E-L equation.

$$\frac{d^2P_z}{dz^2} = [2\alpha_2 P_z + 4\alpha_4 P_z^3 + 6\alpha_6 P_z^5 + 8\alpha_8 P_z^7 - E_z]/\gamma \quad (7)$$

The intrinsic variation in polarization near the surface leads to the following boundary conditions [57];

$$\frac{dP_z}{dz} = \pm\frac{P_z}{\delta} \; at \; z = \mp L/2 \quad (8)$$

We adopt the gradient coefficient γ as 1 nm [59]. The extrapolation length δ = 4 nm used in this study is adopted from earlier phenomenological analyses of BFO thin films [59] and is kept fixed for all calculations. Physically, δ characterizes the strength of surface-induced suppression of polarization: smaller δ corresponds to stronger surface effects, which tend to increase the critical thickness, whereas larger δ weakens surface suppression and can reduce the critical thickness. The magnitude of polarization along the space diagonal in the rhombohedral structure of BFO, can be calculated as $P^2 = P_x^2 + P_y^2 + P_z^2 = 3P_z^2$. Therefore, the total volume bulk energy Eq. (6) is given by

$$G_{bulk} = \alpha_1P^2 + \frac{1}{3}(\alpha_{11} + \alpha_{12})P^4 + \frac{1}{27}(3\alpha_{111} + 6\alpha_{112} + \alpha_{123})P^6 + \frac{1}{81}(3\alpha_{1111} + 6\alpha_{1112} + 3\alpha_{1122} + 3\alpha_{1123})P^8 \quad (9)$$

By differentiating the total free energy Eq. (1) with respect to P_z at a constant temperature T, in the absence of an external field, yields the dielectric equation of state. This equation describes the effect of applying an external electric field to the ferroelectric BFO film.

$$E_z = \int_{-\frac{L}{2}}^{\frac{L}{2}}[2\alpha_2 P_z + 4\alpha_4 P_z^3 + 6\alpha_6 P_z^5 + 8\alpha_8 P_z^7]\, dz \quad (10)$$

The dielectric hysteresis loops shown in Figs. 5 and 6 are obtained by solving the equation of state Eq. (10) under a quasi-static cycling electric field. For each value of the applied field, the equilibrium polarization was determined using a fourth-order Runge–Kutta integration of the E-L equation, combined with an iterative procedure to achieve self-consistency between the polarization profile and the applied field. The field was swept from negative to positive values and back, and the corresponding polarization values were recorded to construct the dielectric hysteresis loop.

The response of the order parameter, polarization, to an external electric field in ferroelectrics is quantified by the dielectric susceptibility, χ. The dielectric susceptibility is given by $\chi = \frac{1}{\varepsilon_0}\frac{\partial P_z}{\partial E_z}$ while its inverse is $\chi^{-1} = \varepsilon_0\frac{\partial E_z}{\partial P_z}$. For temperatures below the transition temperature, the inverse susceptibility can be calculated by:

$$\chi^{-1} = \int_{-\frac{L}{2}}^{\frac{L}{2}}\varepsilon_0[2\alpha_2 + 12\alpha_4 P_z^2 + 30\alpha_6 P_z^4 + 56\alpha_8 P_z^6]\, dz \quad (11)$$

The numerical method for obtaining the calculations proceeds as follows: Assuming the polarization profile is symmetrical with respect

to the film center (at $z = 0$), the surface polarizations P_{-z} and P_{+z} are equal, and the polarization at the film center can be denoted as $P_z\,(z = 0) = P_{zc}$. Consequently, the slope of the polarization profile dP_z/dz is zero at $z = 0$. The numerical procedure starts by determining the equilibrium polarization of the film, which is obtained using the fourth-order Runge-Kutta routine [60] to integrate the E-L equation (Eq. 7) for $E_z = 0$ from $z = -L/2$ to $z = L/2$. The integration of the E-L equation is subject to the boundary conditions outlined in Eq. (8).

3. Results and Discussion

Based on Eq. (7) and Eq. (8) with $E_z = 0$, Fig. 1 shows the equilibrium polarization profile P_z of the BFO film with a positive extrapolation length δ = 4 nm, for different film thicknesses L = 0.5, 1, 2, 4, and 6 nm, at a temperature of T = 20 °C. It is evident that the polarization is suppressed at the film surfaces, and as the film thickness L increases, both surface and interior polarizations rise. Fig. 2 illustrates the variation of average polarization with film thickness at T = 20 °C. The spontaneous polarization diminishes to zero at a certain critical thickness, where the film loses its ferroelectric properties. From Fig. 2, the critical thickness (driven thickness phase transition) of BFO is determined to be 0.452 nm. This critical thickness marks the point at which the film is too thin to sustain ferroelectricity, and is a key parameter in thin films because it defines the minimum thickness required for a material to exhibit ferroelectric behavior. Considering the atomic spacing of the BFO unit cell, with lattice constants of a_{hex} = 5.58 Å and c_{hex} = 13.9 Å at room temperature [61], this implies that even a single unit cell of BFO retains ferroelectricity based on our predicted critical thickness.

Although the theoretical critical thickness obtained here is 0.452 nm, experimentally grown ultrathin BFO films typically have thicknesses in the range of ≥ 2. Our model predicts a finite, non-negligible polarization for 1–2 nm films (see Figs. 1–3), which is consistent with experimental observations of stable ferroelectricity in BFO films down to about 2 nm, grown on conductive perovskite substrates [62]. In this sense, the calculated critical thickness represents an intrinsic lower bound for ferroelectric stability, while experimentally accessible thicknesses of ≥1–2 nm are expected to remain ferroelectric in agreement with these reports.

It is important to note that the present calculations are performed for a freestanding, stress-free BFO film. This assumption allows us to isolate the intrinsic size effect on polarization without the influence of epitaxial strain. In experimental systems, however, BFO films are usually grown on substrates where misfit strain (compressive or tensile) can significantly alter the polarization profile and transition temperature. Compressive strain typically enhances out-of-plane polarization and increases Tc, potentially reducing the critical thickness, whereas tensile strain suppresses it, leading to a larger effective critical thickness. Therefore, the trends shown in Figs. 1 and 2 represent the intrinsic limit of size-driven polarization suppression, in the absence of strain.

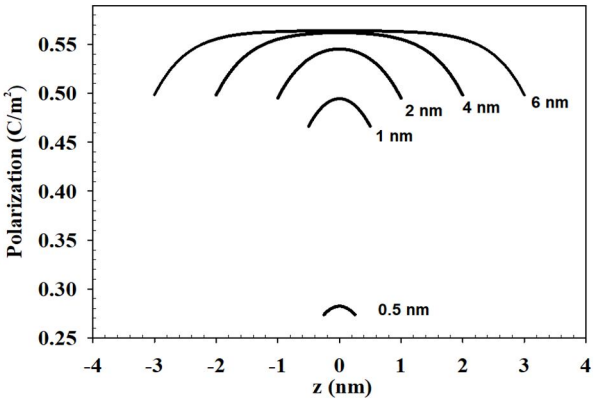

FIG. 1. Polarization P_z as a function of z for BFO films with various thicknesses L = 0.5, 1, 2, 4, and 6 nm. The calculations are performed with a positive extrapolation length δ = 4 nm, gradient coefficient γ = 1 nm, temperature T = 20 °C, and E_z = 0.

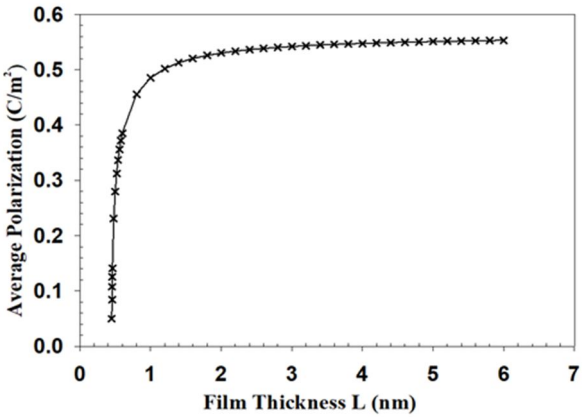

FIG. 2. Average polarization as a function of film thickness L for BFO films at T = 20 °C, E_z = 0, with extrapolation length δ = 4 nm, and gradient coefficient γ = 1 nm.

Figure 3 shows the temperature dependence of the polarization for BFO films with thicknesses L = 0.5, 1, 2, 4, and 6 nm, and bulk BFO, under zero applied electric field. For the Landau coefficients used in this work, the theoretical bulk transition temperature of BFO is approximately 830 °C. The 6 nm film exhibits a transition temperature of about 780 °C, which is therefore ~50 °C lower than the theoretical bulk value. Thinner films show a stronger size-dependent suppression of T(C): the 2 nm and 1 nm films lose their polarization at approximately 658 °C and 472 °C, respectively, as shown in Fig. 3. The 0.5 nm film becomes paraelectric at around 100 °C, consistent with its strong finite-size suppression. The qualitative trend—an increase of T(C) with thickness—is fully consistent with experimental observations. Simultaneously, the average polarization decreases as the film thickness decreases. As the temperature approaches the transition point, the average polarization of the films decreases continuously, indicating a second-order phase transition to the paraelectric phase. In our calculations, we used the standard Landau coefficients from the literature, as detailed in Table A1. Specifically, the fourth-order terms, α_{11} and α_{12}, contribute to determining the order of the transition. When these coefficients are combined, they yield an effective fourth-order term that is positive in our calculations. This positive value indicates a continuous transition, consistent with a second-order phase transition, despite experimental studies suggesting a first-order transition of BFO bulk at approximately 825° C. This suggests that BFO thin films can be fabricated with substantial polarization and a transition temperature well above room temperature.

Figure 4 shows the average polarization versus temperature T for a BFO film with a thickness of L = 4 nm, under different applied electric fields E = 0.0, 0.1 × 10^8, 0.5 × 10^8, and 1.0×10^8 V/m. In the absence of an applied field, the system exhibits a second-order phase transition at the critical temperature. However, when an external electric field is applied, the phase transition is suppressed. As the applied field increases, the average polarization at a given temperature also increases.

Dielectric hysteresis loops (DHL) of BFO films, calculated using Eq. (10), are presented in Fig. 5 for various film thicknesses L = 0.5, 1, and 4 nm at T = 20 $°C$. The results show that as the film thickness increases, both the remnant polarization and coercive field also increase. Fig. 6 illustrates the DHL at different temperatures. As the temperature rises, the area of the DHL decreases, which is attributed to the reduction in remnant polarization and coercive field.

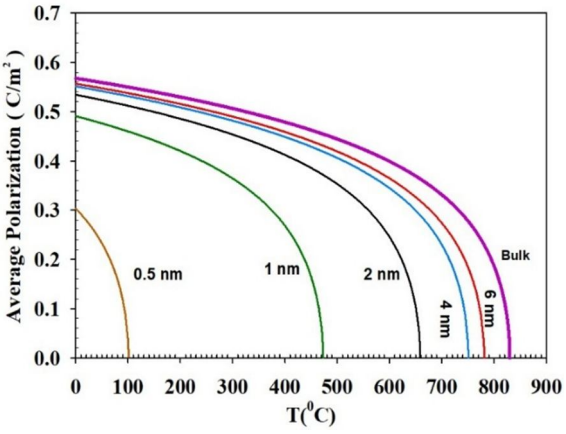

FIG. 3. Temperature dependence of average polarization for bulk and various film thickness $L = 0.5, 1, 2, 4,$ and 6 nm, δ = 4 nm, $\gamma = 1$ nm.

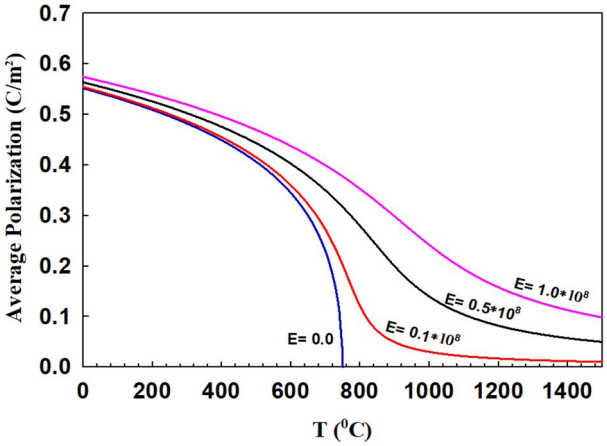

FIG. 4. Polarization versus temperature for BFO film with several applied electric fields $E = 0.0, 0.1 \times 10^8, 0.5 \times 10^8$ and 1.0×10^8 V/m. Film thickness = 4 nm, $\delta = 4$ nm $\gamma = 1$ nm.

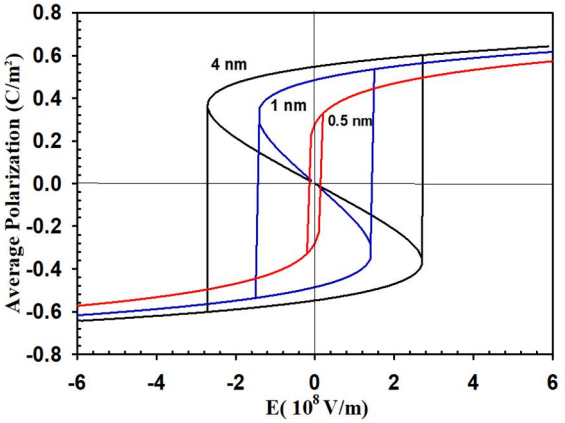

FIG. 5. Dielectric hysteresis loop for BFO films with varying thicknesses L = 0.5,1, and 4 nm at T = 20 °C, with gradient coefficient γ = 1 nm and extrapolation length δ = 4 nm.

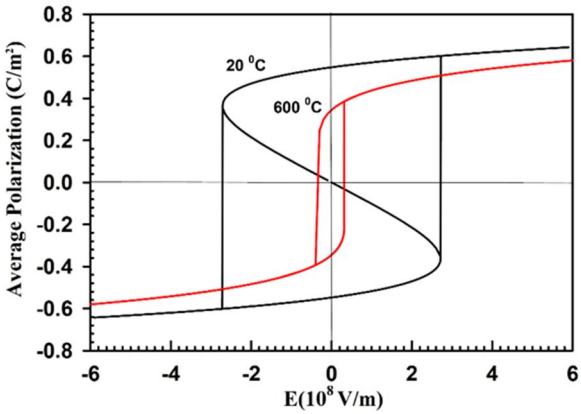

FIG. 6. Dielectric hysteresis loop for a BFO film with thickness L = 4 nm, at temperatures T = 20 °C and 600 °C, with gradient coefficient γ = 1 nm and extrapolation length δ = 4.

Although Fig. 5 presents representative results for the 0.5 nm, 1 nm, and 4 nm films, the same qualitative behavior is observed for all the other studied thicknesses (2 nm, 6 nm, and bulk). These particular thicknesses were selected as illustrative examples, and the general trend is valid across the entire thickness range considered in this work.

Figure 7 illustrates the temperature dependence of the electric susceptibility of BFO films with various thicknesses (L = 1, 2, and 4 nm). Above the transition temperature, the susceptibility is determined using the well-known Curie-Weiss law, while below the transition temperature, Eq. (11) is applied. Peaks in the susceptibility curves correspond to the transition temperatures (T_C) for each film, as indicated in Fig. 3. The portion of the curves above T_C has a clear physical significance, as it can be experimentally observed in the paraelectric phase. Notably, the susceptibility at the transition temperatures increases sharply, reaching values as high as 10^4. A closer look at Fig. 7 (inset) reveals that at room temperature, the thinner films exhibit higher susceptibility, with a value of 51.7 at T = 30°C. This finding aligns with experimental results by J. Lu et al. [63], who reported an average dielectric constant (ε) of approximately 50 in low-temperature dielectric measurements on small BFO single crystals.

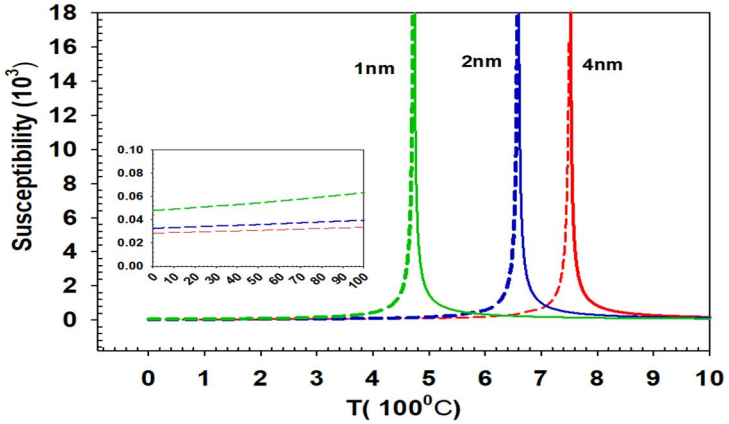

FIG. 7. Dielectric susceptibility versus temperature for BFO films with different thicknesses (1 nm, 2 nm, and 4 nm) at γ = 1 nm and δ = 4 nm. The inset provides a zoomed-in view of the susceptibility of the films at low temperatures below the transition temperatures.

4. Conclusion

In conclusion, we applied Landau theory to examine the intrinsic dielectric properties of freestanding BFO thin films. The study examines dielectric hysteresis loops at varying temperatures and film thicknesses. Our findings indicate that both coercive fields and remnant polarization decrease with reduced film thickness and increased temperature. The critical

thickness of BFO was determined to be 0.452 nm, suggesting the feasibility of fabricating monolayer BFO with ferroelectric properties. We also calculated the susceptibility of BFO under different film thicknesses, yielding a value of ε = 51.7 at room temperature, which aligns closely with experimental data. Additionally, the transition temperature of BFO was found to be thickness-dependent, decreasing with reduced film thickness but remaining above room temperature even for films as thin as 0.5 nm. This size- and temperature-dependent behavior of BFO thin films, as presented here, could guide the design and fabrication of nanoscale ferroelectric devices with tailored properties for advanced applications in electronics and spintronics.

Conflict of Interests:

The authors declare no conflicts of interest.

Data Availability Statement:

No data were generated or analyzed in this study. Data associated with this article cannot be disclosed due to legal, ethical, or other reasons.

Funding:

A-B M. A. Ibrahim acknowledges the financial support provided by the Malaysia Ministry of Higher Education (MOHE) under the national grant FRGS/1/2021/STG07/UITM/02/10.

Acknowledgments

Ahmad Alrub is grateful to Al-Hussein Bin Talal University in Jordan, specifically the College of Science, Physics Department, for providing the facilities used in this work.

The Authors' Contribution Statement:

Conceptualization: Ahmad Musleh Alrub and Abdel-Baset M. A. Ibrahim; Methodology: Ayat M. AlSiedat; Software: Emad A. M. Farrag; Validation: J. M. Khoshman, Hatem A. Al Ameryeen; Formal Analysis: Ahmad Musleh Alrub; Investigation: Bilal Abdallah Sadeh; Writing – Original Draft Preparation: Ahmad Musleh Alrub and Abdel-Baset M. A. Ibrahim; Writing – Review & Editing: J. M. Khoshman and Hatem A. Al Ameryeen; Visualization: Bilal Abdallah Sadeh; Supervision: Ahmad Musleh Alrub; Project Administration: Ahmad Musleh Alrub; Funding Acquisition: Abdel-Baset M. A. Ibrahim.

Appendix A

Table A1: The value of Landau coefficients of energy function in Eq. (5)

coefficient	Value	Unit
α_1	4.483 × (T- 830) x 10^5	(C^{-2} m^2 N)
α_{11}	2.217 × 10^9	(C^{-4} m^6 N)
α_{12}	-2.049 × 10^9	(C^{-4} m^6 N)
α_{111}	-1.760 × 10^9	(C^{-6} m^{10} N)
α_{112}	8.298 × 10^8	(C^{-6} m^{10} N)
α_{123}	1.679 × 10^9	(C^{-6} m^{10} N)
α_{1111}	3.920 × 10^8	(C^{-8} m^{14} N)
α_{1112}	4.400 × 10^7	(C^{-8} m^{14} N)
α_{1122}	-3.800 × 10^8	(C^{-8} m^{14} N)
α_{1123}	8.000 × 10^8	(C^{-8} m^{14} N)

Table A2: The value of Landau coefficients of the energy function in Eq. (6)

Coefficient	Value	Unit
α_2	13.449 × (T- 830) x 10^5	(C^{-2} m^2 N)
α_4	5.600 × 10^7	(C^{-4} m^6 N)
α_6	5.100 × 10^7	(C^{-6} m^{10} N)
α_8	3.330 × 10^7	(C^{-8} m^{14} N)

References

[1] Gumiel, C. and Calatayud, D.G., Boletín de la Sociedad Española de Cerámica y Vidrio, 61 (6) (2022) 708.

[2] Shvartsman, V.V., Kleemann, W., Haumont, R., and Kreisel, J., Applied Physics Letters, 90 (17) (2007).

[3] Lebeugle, D., Colson, D., Forget, A., and Viret, M., Applied Physics Letters, 91 (2) (2007).

[4] Neaton, J.B., Ederer, C., Waghmare, U.V., Spaldin, N.A., and Rabe, K.M., Physical Review B, 71 (1) (2005) 014113.

[5] Ravindran, P., Vidya, R., Kjekshus, A., Fjellvåg, H., and Eriksson, O., Physical Review B, 74 (22) (2006) 224412.

[6] Wang, Y.P., Yuan, G.L., Chen, X.Y., Liu, J.M., and Liu, Z.G., Journal of Physics D: Applied Physics, 39 (10) (2006) 2019.

[7] Pradhan, A.K., Zhang, K., Hunter, D., Dadson, J.B., Loiutts, G.B., Bhattacharya, P., Katiyar, R., Zhang, J., Sellmyer, D.J., Roy, U.N., Cui, Y., and Burger, A., Journal of Applied Physics, 97 (9) (2005) 093903.

[8] Selbach, S.M., Einarsrud, M.A., and Grande, T., Chemistry of Materials, 21 (1) (2009) 169.

[9] Bernardo, M.S., Jardiel, T., Peiteado, M., Caballero, A.C., and Villegas, M., Journal of the European Ceramic Society, 31 (16) (2011) 3047.

[10] Bernardo, M.S., Jardiel, T., Peiteado, M., and Caballero, A.C., Journal of the Ceramic Society of Japan, 124 (1) (2016) 92.

[11] Yang, C.H., Kan, D., Takeuchi, I., Nagarajan, V., and Seidel, J., Physical Chemistry Chemical Physics, 14 (46) (2012) 15953.

[12] Arnold, D.C., IEEE Transactions on Ultrasonics, Ferroelectrics, and Frequency Control, 62 (1) (2015) 62.

[13] Catalan, G. and Scott, J.F., Advanced Materials, 21 (24) (2009) 2463.

[14] Kan, D., Long, C.J., Steinmetz, C., Lofland, S.E., and Takeuchi, I., Journal of Materials Research, 27 (21) (2012) 2691.

[15] Ederer, C. and Spaldin, N.A., Physical Review Letters, 95 (25) (2005) 257601.

[16] Ricinschi, D., Yun, K.Y., and Okuyama, M., Journal of Physics: Condensed Matter, 18 (6) (2006) L97.

[17] Kartavtseva, M.S., Gorbenko, O.Y., Kaul, A.R., Murzina, T.V., Savinov, S.A., and Aktsipetrov, O.A., Journal of Materials Research, 22 (8) (2007) 2063.

[18] Bennett, C.J., Kim, H.S., Varela, M., Biegalski, M.D., Kim, D.H., Norton, D.P., Meyer, H.M., and Christen, H.M., Journal of Materials Research, 26 (10) (2011) 1326.

[19] Wang, J., Neaton, J.B., Zheng, H., Nagarajan, V., Ogale, S.B., Liu, B., Viehland, D., Vaithyanathan, V., Schlom, D.G., Waghmare, U.V., Spaldin, N.A., Rabe, K.M., Wuttig, M., and Ramesh, R., Science, 299 (5613) (2003) 1719.

[20] Yang, S.Y., Seidel, J., Byrnes, S.J., Shafer, P., Yang, C.H., Rossell, M.D., Yu, P., Chu, Y.H., Scott, J.F., Ager, J.W., Martin, L.W., and Ramesh, R., Nature Nanotechnology, 5 (2) (2010) 143.

[21] Yang, J.C., He, Q., Yu, P., and Chu, Y.H., Annual Review of Materials Research, 45 (1) (2015) 249.

[22] Ramesh, R. and Spaldin, N.A., Nature Materials, 6 (1) (2007) 21.

[23] Gupta, S., Pal, M., Tomar, M., Guo, R., Bhalla, A., and Gupta, V., Journal of Alloys and Compounds, 882 (2021) 160698.

[24] González-Abreu, Y., Reis, S.P., Freitas, F.E., Eiras, J.A., and Araújo, E.B., Journal of Advanced Dielectrics, 11 (3) (2021) 2140007.

[25] Martin, L.W., Crane, S.P., Chu, Y.H., Holcomb, M.B., Gajek, M., Huijben, M., Yang, C.H., Balke, N., and Ramesh, R., Journal of Physics: Condensed Matter, 20 (43) (2008) 434220.

[26] Zeches, R.J., Rossell, M.D., Zhang, J.X., Hatt, A.J., He, Q., Yang, C.H., Kumar, A., Wang, C.H., Melville, A., Adamo, C., Sheng, G., Chu, Y.H., Ihlefeld, J.F., Erni, R., Ederer, C., Gopalan, V., Chen, L.Q., Schlom, D.G., Spaldin, N.A., Martin, L.W., and Ramesh, R., Science, 326 (5955) (2009) 977.

[27] Hatt, A.J., Spaldin, N.A., and Ederer, C., Physical Review B, 81 (5) (2010) 054109.

[28] Damodaran, A.R., Liang, C.W., He, Q., Peng, C.Y., Chang, L., Chu, Y.H., and Martin, L.W., Advanced Materials, 23 (28) (2011) 3170.

[29] Kumari, A., Kumari, K., Ahmed, F., Ahmad, M.M., Sharma, J., Vij, A., and Kumar, S., Journal of Materials Science: Materials in Electronics, 32 (19) (2021) 23968.

[30] Miranda, H., de Obaldía, E., and Ching-Prado, E., International Engineering, Sciences and Technology Conference (IESTEC), (2022) 802.

[31] Parveen, A., Abbas, Z., Hussain, S., Shaikh, S.F., Aslam, M., and Jung, J., Micromachines, 14 (12) (2023) 2251.

[32] Tariq, M., Shaari, A., Chaudhary, K., Jalil, A., Ismail, F.D., Ahmed, R., and Ehsan, S.A., Materials Science and Engineering: B, 300 (2024) 117070.

[33] Alrub, A.M., Anbar, A.A., and Ibrahim, A.B., AIP Advances, 14 (6) (2024).

[34] Alrub, A.M., Journal of Applied Physics, 126 (15) (2019) 154102.

[35] Pertsev, N.A., Zembilgotov, A.G., and Tagantsev, A.K., Physical Review Letters, 80 (9) (1998) 1988.

[36] Ban, Z.G. and Alpay, S.P., Journal of Applied Physics, 91 (11) (2002) 9288.

[37] Zembilgotov, A.G., Pertsev, N.A., Böttger, U., and Waser, R., Applied Physics Letters, 86 (5) (2005).

[38] Daraktchiev, M., Catalan, G., and Scott, J.F., Physical Review B, 81 (22) (2010) 224118.

[39] Vanderbilt, D. and Cohen, M.H., Physical Review B, 63 (9) (2001) 094108.

[40] Moreau, J.-M., Michel, C., Gerson, R., and James, W.J., Journal of Physics and Chemistry of Solids, 32 (6) (1971) 1315.

[41] Kubel, F. and Schmid, H., Acta Crystallographica Section B, 46 (6) (1990) 698.

[42] Palai, R., Katiyar, R.S., Schmid, H., Tissot, P., Clark, S.J., Robertson, J., Redfern, S.A.T., Catalan, G., and Scott, J.F., Physical Review B, 77 (1) (2008) 014110.

[43] Polomska, M., Kaczmarek, W., and Pająk, Z., Physica Status Solidi, 23 (2) (1974) 567.

[44] Haumont, R., Kreisel, J., and Bouvier, P., Phase Transition, 79 (12) (2006) 1043.

[45] Kornev, I.A., Lisenkov, S., Haumont, R., Dkhil, B., and Bellaiche, L., Physical Review Letters, 99 (22) (2007) 227602.

[46] Haumont, R., Kornev, I.A., Lisenkov, S., Bellaiche, L., Kreisel, J., and Dkhil, B., Physical Review B, 78 (13) (2008) 134108.

[47] Watanabe, Y., Physical Review B, 57 (2) (1998) 789.

[48] Nelson, C.T., Winchester, B., Zhang, Y., Kim, S.J., Melville, A., Adamo, C., Folkman, C.M., Baek, S.H., Eom, C.B., Schlom, D.G., Chen, L.Q., and Pan, X., Nano Letters, 11 (2) (2011) 828.

[49] Béa, H., Bibes, M., Barthélémy, A., Bouzehouane, K., Jacquet, E., Khodan, A., Contour, J.P., Fusil, S., Wyczisk, F., and Forget, A., Applied Physics Letters, 87 (7) (2005).

[50] Fennie, C.J., Physical Review Letters, 100 (16) (2008) 167203.

[51] Kadomtseva, A.M., Zvezdin, A.K., Popov, Yu. F., Pyatakov, A.P., and Vorob'ev, G.P., Journal of Experimental and Theoretical Physics Letters, 79 (11) (2004) 571.

[52] Wang, N., Cheng, J., Pyatakov, A.P., Zvezdin, A.K., Li, J.F., Cross, L.E., and Viehland, D., Physical Review B, 72 (10) (2005) 104434.

[53] Bai, F., Wang, J., Wuttig, M., Li, J., Wang, N., Pyatakov, A.P., Zvezdin, A.K., Cross, L.E., and Viehland, D., Applied Physics Letters, 86 (3) (2005).

[54] Tilley, D.R. and Žekš, B., Solid State Communications, 49 (8) (1984) 823.

[55] Alrub, A.M. and Ong, L.H., European Physical Journal B, 88 (1) (2015) 9.

[56] Peng, R.C., Cheng, X., Peng, B., Zhou, Z., Chen, L.Q., and Liu, M., Acta Materialia, 208 (2021) 116689.

[57] Kretschmer, R. and Binder, K., Physical Review B, 20 (3) (1979) 1065.

[58] Haun, M.J., Furman, E., Jang, S.J., and Cross, L.E., Ferroelectrics, 99 (1) (1989) 13.

[59] Glinchuk, M.D., Morozovska, A.N., Eliseev, E.A., and Blinc, R., Journal of Applied Physics, 105 (8) (2009) 084108.

[60] Press, W.H., Flannery, B.P., Teulosky, S.A., and Vetterling, W.T., Numerical Recipes in Fortran 77, in The Art of Scientific Computing, (Cambridge University Press, Cambridge, 1997).

[61] Kadomtseva, A.M., Popov, Yu.F., Pyatakov, A.P., Vorob'ev, G.P., Zvezdin, A.K., and Viehland, D., Phase Transition, 79 (12) (2006) 1019.

[62] Feng, Y., Wang, C., Tian, S., Zhou, Y., Ge, C., Guo, H., He, M., Jin, K., and Yang, G., Nanotechnology, 27 (2016) 355604.

[63] Lu, J., Günther, A., Schrettle, F., Mayr, F., Krohns, S., Lunkenheimer, P., Pimenov, A., Travkin, V.D., Mukhin, A.A., and Loidl, A., The European Physical Journal B, 75 (4) (2010) 451.